Electronic Supplementary Material (ESI) for Journal of Materials Chemistry B.


# Supplementary Information

## Supramolecular assemblies of histidine-containing peptides with switchable hydrolase and peroxidase activities through Cu (II) binding and co-assembling

Yue Zhang,[a] Xin Tian,[*b] and Xinming Li[*a]

[a.] College of Chemistry, Chemical Engineering and Materials Science, Soochow University, Suzhou 215123, China.

[b.] State Key Laboratory of Radiation Medicine and Protection, School for Radiological and Interdisciplinary Sciences (RAD-X), Soochow University, Suzhou, 215123, China.

Email: xinmingli@suda.edu.cn; xtian@suda.edu.cn.

## Contents

## 1. Materials and methods

2-chlorotrityl chloride resin, Fmoc-His(Trt)-OH, Fmoc-Arg(Pbf)-OH, Fmoc-Lys(Boc)-OH, Fmoc-Asp(OtBu)-OH, Fmoc-Ser(tBu)-OH, Fmoc-Phe-OH and o-benzotriazol-1-yl-tetramethyluronium hexafluorophosphate (HBTU) were purchased from GL Biochem (Shanghai, China). 2-(naphthalen-6-yl) acetic acid was provided by Aladdin (Shanghai, China). Piperidine, trifluoroacetic acid (TFA) and *N,N*-diisopropylethylamine (DIEA) were from Energy Chemical and Adamas, respectively. 10 mM phosphate buffered solution was obtained by Sangong Bioengineering (Shanghai, China). *p*-nitrophenol acetate and *p*-nitrophenol were provided by Shanghai Aladdin Biochemical Technology. $CuCl_2 \cdot 2H_2O$ and other metal compounds was provided by Sinopharm Chemical Reagent (Suzhou, China). Superoxide dismutase was supplied by Shanghai Yuanye Biotechnology. Horse radish peroxidase (300 unit/mg) was provided by Shanghai Baoman Biological Technology. Proteinase from *aspergillus melleus* ($\geq$ 3.0 unit/mg) was purchased from Sigma-Aldrich. 3,3',5,5'-tetramethylbenzidine (TMB) was provided by Macklin and tertiary butanol were purchased from Aladdin. $^1$H NMR spectra were recorded on the Unity Inova 400 MHz by using DMSO-*d*6 as the solvent. MALDI-TOF mass spectrometry analysis was conducted on the Bruker Ultraflex-Treme mass spectrometer (Germany). Rheological tests were performed on the Thermo Scientific HAAKE RheoStress 6000 rheometer (Germany). Circular dichroism spectra (CD) were collected from the JASCO J-810 spectrometer (Japan). Fourier transform infrared spectroscopy (FTIR) characterizations were carried out on the PerkinElmer spectrophotometer (USA). Transmission electron micrograph (TEM) images were recorded on the Hitachi HT7700 TEM. UV-Vis spectroscopy analysis was performed on the UV-1900i (Shimadzu (Suzhou) Instrument Co. LTD, China). Fluorescence spectra were obtained from F-2700 fluorescence spectrophotometer (Japan) and BioTek Synergy Neo microplate reader. High Performance Liquid Chromatography (HPLC) analysis were conducted on a Waters 2489 with UV/Visible Detector by using $CH_3CN$ (0.1% of TFA) and $H_2O$ (0.1% of TFA) as eluents.

## 2. Experimental section

2.1 Peptide Synthesis: Histidine-containing peptides were synthesized from corresponding amino acids by using the solid-phase peptide synthesis (SPPS) technique with the application of 2-chlorotrityl chloride resin (100-200 mesh and 1.3-1.8 mmol/g). First, 0.5 g resin was swelled in dry dichloromethane (DCM) with $N_2$ bubbling for 30 min and the swelled resin was washed by dry *N,N*-dimethylformamide (DMF) for five times. Then the DMF solution containing *N,N*-diisopropylethylamine (DIEA) and Fmoc-His(Trt)-OH was added to react for 1.5 h and the resin was washed with dry DMF for four times. Afterward, the blocking solution (16:3:1 of DCM / MeOH / DIEA) was added to quench the unreacted sites on the resin for 10 min, and the resin was rinsed thoroughly with dry DMF. Then the resin was treated with 20 % piperidine (in DMF) for 0.5 h to remove Fmoc-protecting groups, and washed with DMF for four times. The designed molecule was elongated step by step by following standard Fmoc solid phase peptide synthesis protocols, and HBTU was used as a coupling reagent. Ultimately, the synthetic peptide was cleaved from the resin by using cleavage cocktail (TFA: $H_2O$ = 95:5). The final yields of synthetic peptides were about 69 %.

**NapFFH:** $^1$H NMR (400 MHz, DMSO-*d*6): δ 8.73 (s, 1H), 8.43 (d, J = 7.9 Hz, 1H), 8.27 (d, J = 8.4 Hz, 1H), 8.20 (d, J = 8.0 Hz, 1H), 7.88-7.82 (m, 1H), 7.81-7.71 (m, 2H), 7.58 (s, 1H), 7.52-7.43 (m, 2H), 7.28 (s, 1H), 7.23 (d, J = 4.3 Hz, 4H), 7.20-7.12 (m, 7H), 4.60-4.48 (m, 3H), 3.11 (dd, J = 15.2, 5.5 Hz, 2H), 3.05-2.92 (m, 4H), 2.83 (dd, J = 14.0, 9.2 Hz, 1H), 2.70 (dd, J = 13.9, 10.4 Hz, 1H). MS: calcd M = 617.2638, obsd $(M + H)^+$ = 618.276, obsd $(M + Na)^+$ = 640.292.

**NapFFHH:** $^1$H NMR (400 MHz, DMSO-*d*6): δ 8.91 (d, J = 23.8 Hz, 2H), 8.49-8.16 (m, 4H), 7.86-7.82 (m, 1H), 7.78-7.70 (m, 2H), 7.57 (s, 1H), 7.50-7.42 (m, 2H), 7.38 - 7.10 (m, 13H), 4.54 (ddd, J = 19.5, 12.6, 8.4 Hz, 4H), 3.14 (ddd, J = 15.8, 13.0, 5.4 Hz, 2H), 3.07-2.88 (m, 5H), 2.87-2.65 (m, 3H). MS: calcd M = 754.3227, obsd $(M + H)^+$ = 755.298, obsd $(M + Na)^+$ = 777.286.

**NapFFRH:** $^1$H NMR (400 MHz, DMSO-*d*6): δ = 8.40 (d, J=7.6, 1H), 8.26 (ddd, J=24.9, 17.4, 7.9, 3H), 8.11 (d, J=8.0, 1H), 7.89-7.83 (m, 1H), 7.76 (dd, J=14.0, 7.7,

2H), 7.59 (s, 1H), 7.53-7.43 (m, 3H), 7.30-7.05 (m, 10H), 4.62-4.47 (m, 3H), 4.35-4.28 (m, 1H), 3.13-3.01 (m, 4H), 3.00-2.92 (m, 2H), 2.90-2.77 (m, 2H), 2.71 (dd, J=13.9, 10.3, 2H), 1.70 (s, 1H), 1.51 (s, 3H). MS: calcd M = 773.3649, obsd $(M + H)^+$ = 774.533, obsd $(M + Na)^+$ = 796.529.

**NapFFKH:** $^1$H NMR (400 MHz, DMSO-*d*6): δ = 8.88 (s, 1H), 8.25 (ddd, J=39.4, 30.4, 8.0, 4H), 7.85 (d, J=7.2, 1H), 7.76 (dd, J=13.8, 7.9, 4H), 7.58 (s, 1H), 7.47 (tt, J=12.4, 6.2, 2H), 7.36 (s, 1H), 7.25-7.11 (m, 10H), 4.53 (ddd, J=18.4, 13.4, 6.1, 3H), 4.25 (dd, J=13.5, 8.0, 1H), 3.16 (dd, J=15.3, 5.2, 2H), 3.06-2.99 (m, 2H), 2.98-2.87 (m, 2H), 2.75 (ddd, J=36.2, 14.1, 10.0, 4H), 1.70-1.46 (m, 4H), 1.30 (s, 2H). MS: calcd M = 754.3588, obsd $(M + H)^+$ = 746.427, obsd $(M + Na)^+$ = 768.406.

**NapFFDH:** $^1$H NMR (400 MHz, DMSO-*d*6): δ = 8.95 (s, 1H), 8.26 (ddd, *J*=42.5, 38.4, 7.7, 4H), 7.85 (d, *J*=7.2, 1H), 7.75 (dd, *J*=12.9, 7.9, 2H), 7.58 (s, 1H), 7.51-7.41 (m, 2H), 7.36 (d, *J*=16.4, 1H), 7.33-7.09 (m, 11H), 4.59-4.48 (m, 4H), 3.16 (dd, *J*=15.2, 5.0, 1H), 3.07-3.00 (m, 2H), 3.00-2.95 (m, 1H), 2.92 (d, *J*=3.7, 1H), 2.80-2.75 (m, 1H), 2.74 (s, 1H), 2.72-2.63 (m, 2H), 2.55 (d, *J*=8.2, 1H). MS: calcd M = 732.2908, obsd $(M + H)^+$ = 733.374, obsd $(M + Na)^+$ = 755.360.

**NapFFSH:** $^1$H NMR (400 MHz, DMSO-*d*6): δ = 8.93 (s, 1H), 8.34-8.12 (m, 4H), 7.85 (d, J=7.1, 1H), 7.75 (dd, J=13.6, 7.9, 2H), 7.58 (s, 1H), 7.51-7.42 (m, 2H), 7.37 (d, J=15.0, 1H), 7.31-7.10 (m, 10H), 4.67-4.46 (m, 3H), 4.32 (dd, J=12.9, 5.7, 1H), 3.59 (d, J=5.2, 2H), 3.19 (d, J=5.3, 1H), 3.15 (d, J=5.0, 1H), 3.10-2.99 (m, 2H), 2.95 (dd, J=13.8, 3.8, 1H), 2.83-2.77 (m, 1H), 2.74 (t, J=5.2, 1H), 2.72-2.65 (m, 1H). MS: calcd M = 704.2958, obsd $(M + H)^+$ = 705.453, obsd $(M + Na)^+$ = 727.426.

**2.2 TEM Characterizations:** Each peptide sample (5 μL) was placed on a carbon-coated copper grid and then stained with phosphotungstic acid (2.0 % w/v) for 13-15 min. After air-drying, the nanostructures within sample were recorded by the transmission electron microscope (Hitachi HT7700).

**2.3 CD and FTIR Characterizations:** CD spectra were recorded on a Jasco J-810 spectrometer. 25 μL of sample were loaded into a 1 mm thick quartz cell and scanned from 185 nm to 300 nm under $N_2$ atmosphere. FTIR spectra were collected with a PerkinElmer spectrophotometer. The sample was loaded into a KBr cuvette using

deuterium oxide ($D_2O$) as a solvent. All spectra were scanned 64 times over the range of 3500-900 $cm^{-1}$.

**2.4 Rheological Tests:** Rheological properties of hydrogels were tested on the rheometer (Thermo Scientific HAAKE RheoStress 6000) at 25 °C. First, 300 μL of hydrogels were placed on a 20 mm parallel plate. (i) Dynamic strain sweep tests were implemented from 0.1 to 10% strain with a fixed angular frequency at 6.282 rad/s. (ii) Dynamic frequency sweeps was carried out from 0.628 to 628 rad/s at a fixed strain of 1.0 %.

**2.5 Determination of the critical self-assembling concentration of histidine-containing peptides:** A series of histidine-containing peptides solutions with the concentration from 50 to 3000 μg/mL were prepared in PBS buffer. After incubating with Thioflavin T (20 μM) for 12 h in dark, the fluorescence intensities of the peptide solutions containing Thioflavin T were measured on a F-2700 fluorescence spectrophotometer at 25 °C ($\lambda_{ex}$ = 440 nm, $\lambda_{em}$ = 490 nm). The critical self-assembling concentration of peptides was obtained according to the dose-dependent curve plotted with fluorescence intensities of Thioflavin T versus varied concentrations of peptides.

**2.6 Determination of the hydrolase-like activities of self-assembling peptides:** Hydrolysis kinetics was tested by adding different amounts of *p*-NPA into the PBS buffer (pH 7.4 and 10 mM) containing each self-assembling peptide ($1 \times 10^{-4}$ M) and the absorbance at 400 nm was monitored by using a UV-vis spectrophotometer (UV-1900i) at 25 °C. The rate constants for *p*-NPA hydrolysis by different peptides were calculated based on the Michaelis-Menten equation: $v_0 = \frac{V_{max}[S]}{K_M + [S]}$. $v_0$ is the initial velocity; $K_M$ is the Michaelis constant; [$S$] is the concentration of substrate; and $V_{max}$ is the maximal reaction velocity.

**2.7 Preparation of peptide-$Cu^{2+}$ complexes:** Histidine-containing peptides were dissolved in ultrapure water followed by adjustment of pH to 9.0, and then mixed with $Cu^{2+}$ ions. The mixture was subject to sonication together with pH adjustment to produce a uniformly dispersed solution. Ultimately, the solutions were heated in water bath to 60 °C and incubated at room temperature for 0.5 h.

**2.8 Determination of the peroxidase-like catalytic activity:** The peroxidase-like catalytic activity was determined by adding 10 μL of TMB solution ($2 \times 10^{-2}$ M in acetonitrile solution) and 20 μL of $H_2O_2$ (0.25 M) into 930 μL of PBS buffer ($1 \times 10^{-2}$ M, pH 7.4). The mixture was homogenized by vortexing and then was incubated under 25 ℃ in a 10 mm path length quartz cuvette. The reaction was initiated by adding 40 μL of the peptide-$Cu^{2+}$ complexes ($5 \times 10^{-3}$ M). The oxidized product of TMB (oxTMB) was quantified by monitoring the absorbance at 640 nm using a UV-vis spectrophotometer (UV-1900i). The initial reaction rate ($v_0$) for oxTMB production was determined to represent the catalytic activity of the peroxidase mimics.

**2.9 Kinetics Analysis:** The reaction kinetics of the peroxidase mimics were established using a steady-state assay. The initial reaction rate for the reactions was determined by fixing the concentrations of one substrate and changing the other. Kinetic parameters were calculated based on the Michaelis-Menten equation.

**2.10 Determination of reactive oxygen species involved in the process of TMB oxidation:** The reactive oxygen species were determined by adding 20 μL of SOD ($3 \times 10^{-3}$ M in PBS buffer) or 20 μL of TBA (3 M in ultrapure water) to the system of catalytic peptide-$Cu^{2+}$, which contained 10 μL of TMB solution ($2 \times 10^{-2}$ M in acetonitrile solution), and 20 μL of $H_2O_2$ ($5 \times 10^{-2}$ M in ultrapure water) in 910 μL of PBS buffer ($1 \times 10^{-2}$ M, pH 7.4). The mixture was homogenized by vortexing and then was incubated under 25 ℃ in a 10 mm path length quartz cuvette. The reaction was initiated by adding 40 μL of peptide-$Cu^{2+}$ complexes ($5 \times 10^{-3}$ M). The production of oxidized TMB (oxTMB) was quantified by monitoring the absorbance at 640 nm using a UV-vis spectrophotometer (UV-1900i).

**2.11 Biostability tests of peptides and peptide-$Cu^{2+}$ complexes:** peptides or peptide-$Cu^{2+}$ complexes were dissolved in PBS buffer ($1 \times 10^{-2}$ M, pH 7.4) to yield a solution with a concentration at 0.02 wt%, followed by the addition of proteinase K (3.2 units/mL) at 37 ℃. At each specific time, 200 μL of the solution was removed and the contents of the components in the solution were analyzed by High Performance Liquid Chromatography (HPLC).

**2.12 Cell Compatibility:** The compatibility of KH or $KH_{Cu}$ with Human umbilical vein endothelial cells (HUVECs) was evaluated via the CCK-8 kit assay. Briefly, the cells were seeded into 96-well plates at a density of $8 \times 10^3$ cells per well with 90 μL of DMEM medium. After overnight incubation, the cells were treated by KH or $KH_{Cu}$ in different concentrations (10, 20, 50 and 100 μM). Untreated HUVECs were used as controls. After incubated for 24 h, the medium was replaced with CCK-8 solution (100 μL, 10%) and then incubated for 3 h. Finally, the absorbance of the formazan product was measured at 450 nm by using a microplate reader.

## 3. Synthesis and characterizations of peptides

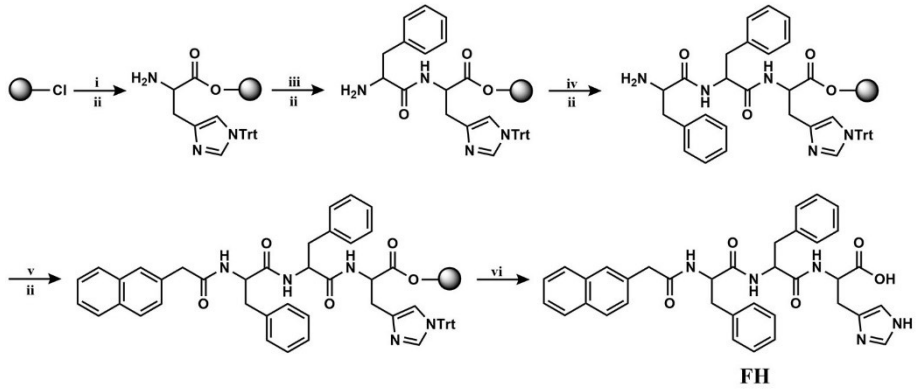

FH

i) Fmoc-His(Trt)-OH, DIEA; ii) 20 % piperidine, DMF; iii) Fmoc-Phe-OH, HBTU, DIEA;
iv) Fmoc-Phe-OH, HBTU, DIEA; v) 2-naphthalene acetic acid, HBTU, DIEA; vi) TFA : water(95 : 5)

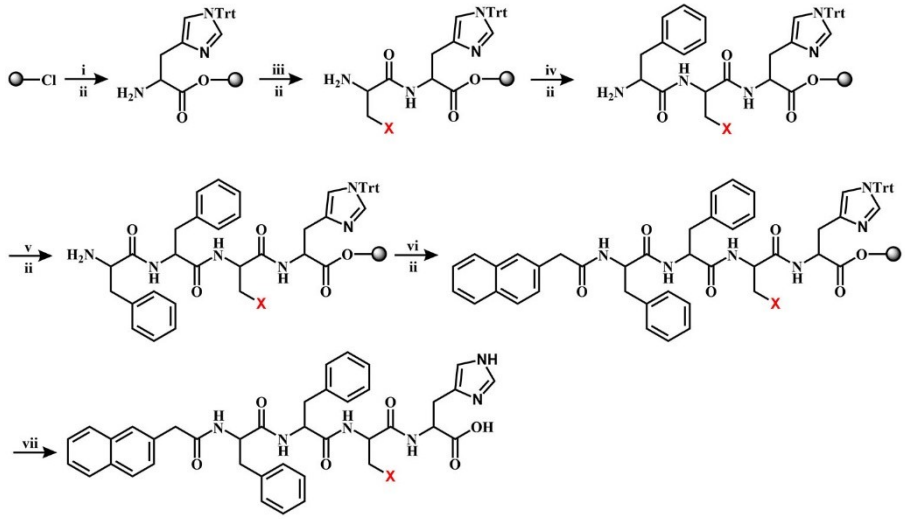

XH

| precursor | HH | RH | KH | DH | SH |
|---|---|---|---|---|---|
| X | 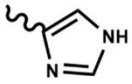 | 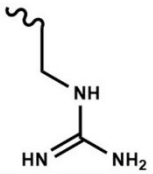 |  | 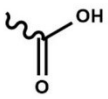 |  |

i) Fmoc-His(Trt)-OH, DIEA; ii) 20 % piperidine, DMF; iii) Fmoc-His(Trt)-OH or Fmoc-Arg(Pbf)-OH
or Fmoc-Lys(Boc)-OH or Fmoc-Asp(OtBu)-OH or Fmoc-Ser(tBu)-OH ,HBTU, DIEA;
iv) Fmoc-Phe-OH, HBTU, DIEA; v) Fmoc-Phe-OH, HBTU, DIEA;
vi) 2-naphthalene acetic acid, HBTU, DIEA; vii) TFA : water (95 : 5)

**Fig. S1.** Synthetic routes for the preparation of histidine-containing peptides.

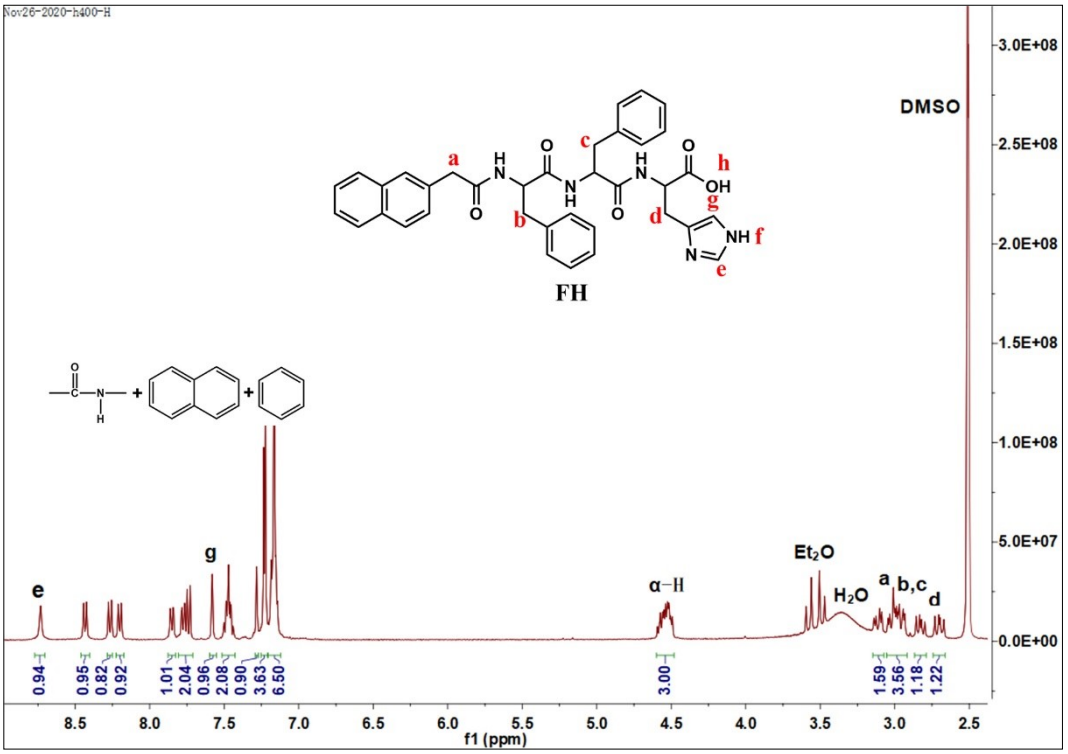


**Fig. S2.** [1]H NMR of FH in DMSO-*d6*.

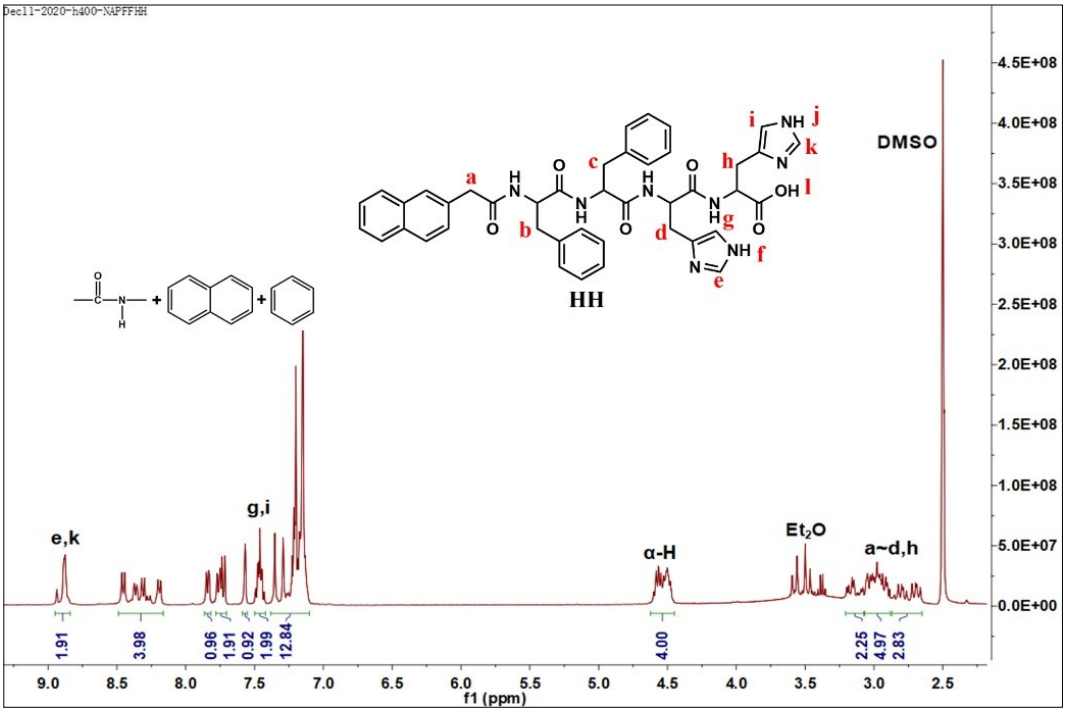


**Fig. S3.** [1]H NMR of HH in DMSO-*d6*.

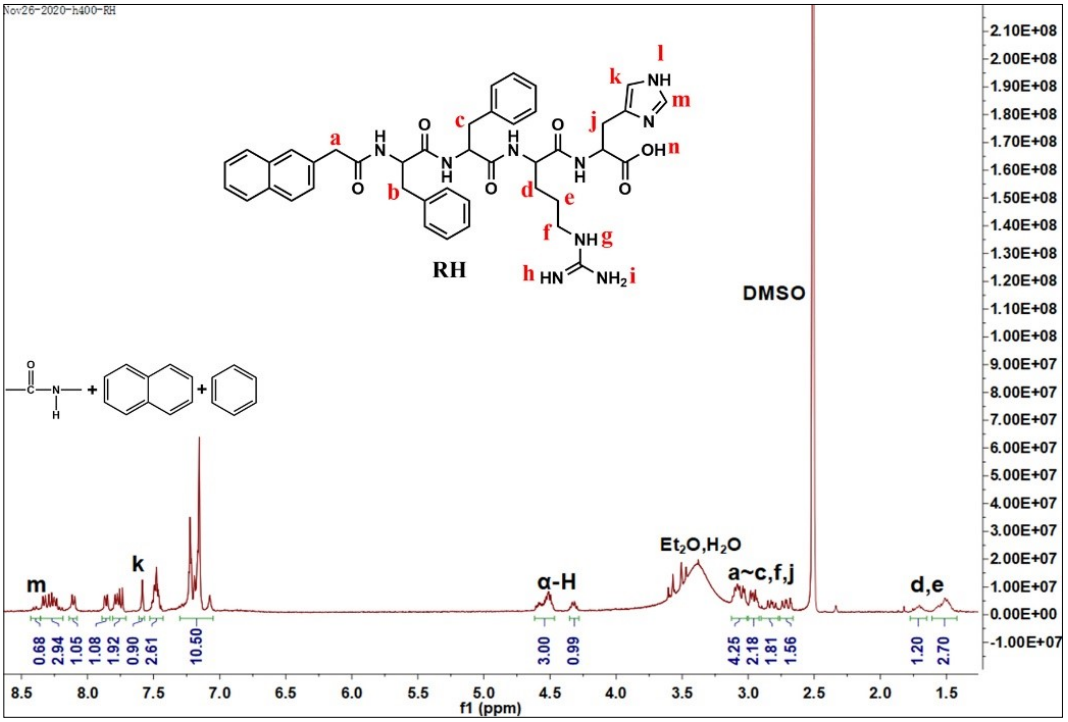


**Fig. S4.** [1]H NMR of RH in DMSO-*d6*.

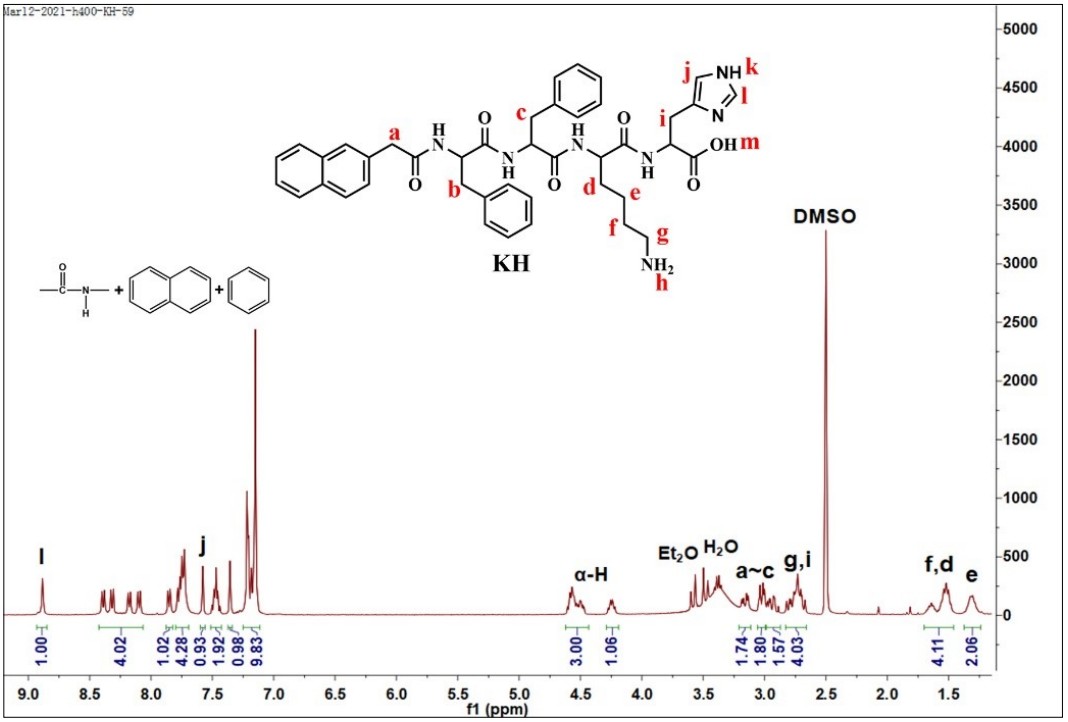


**Fig. S5.** [1]H NMR of KH in DMSO-*d6*.

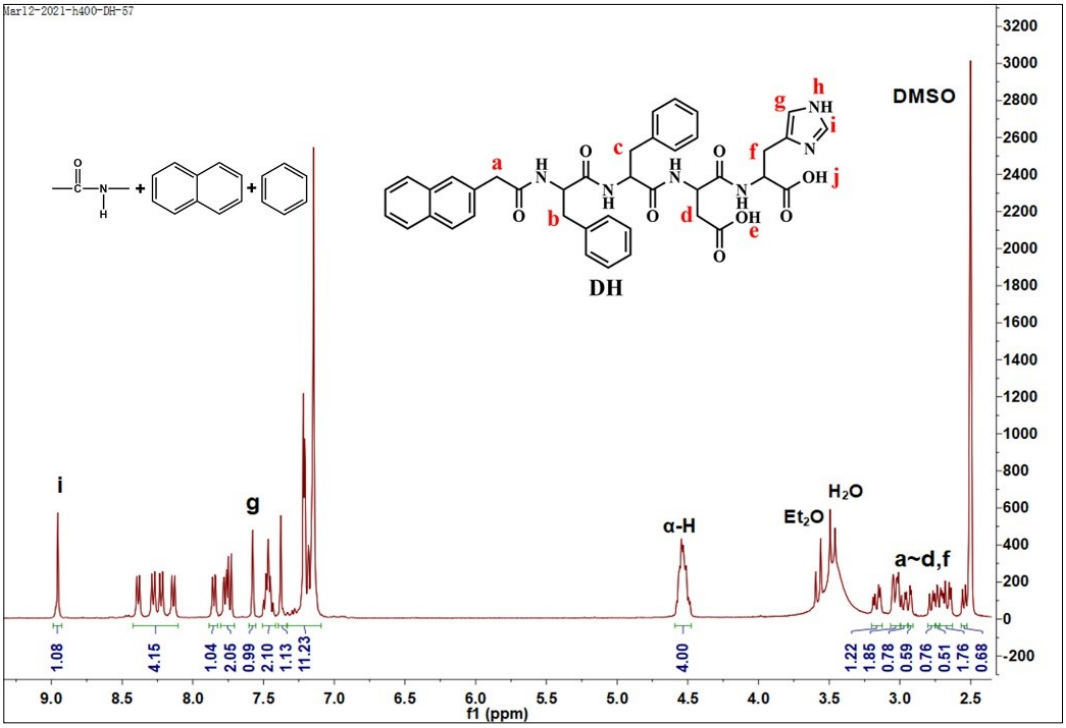


**Fig. S6.** [1]H NMR of DH in DMSO-*d6*.

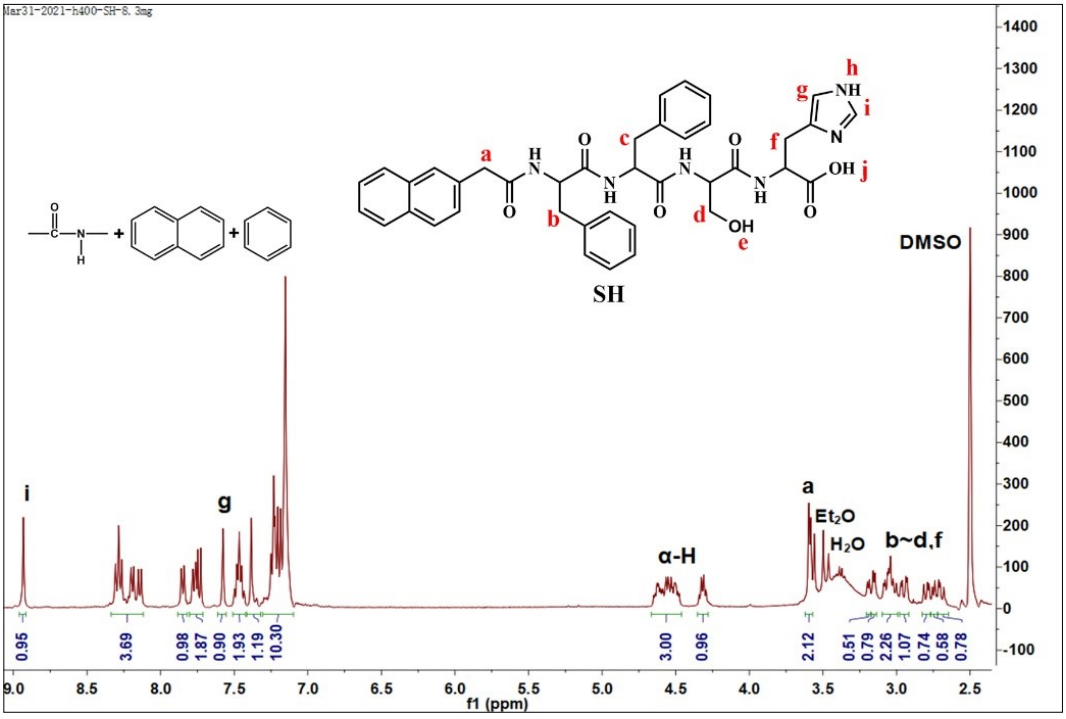


**Fig. S7.** [1]H NMR of SH in DMSO-*d6*.

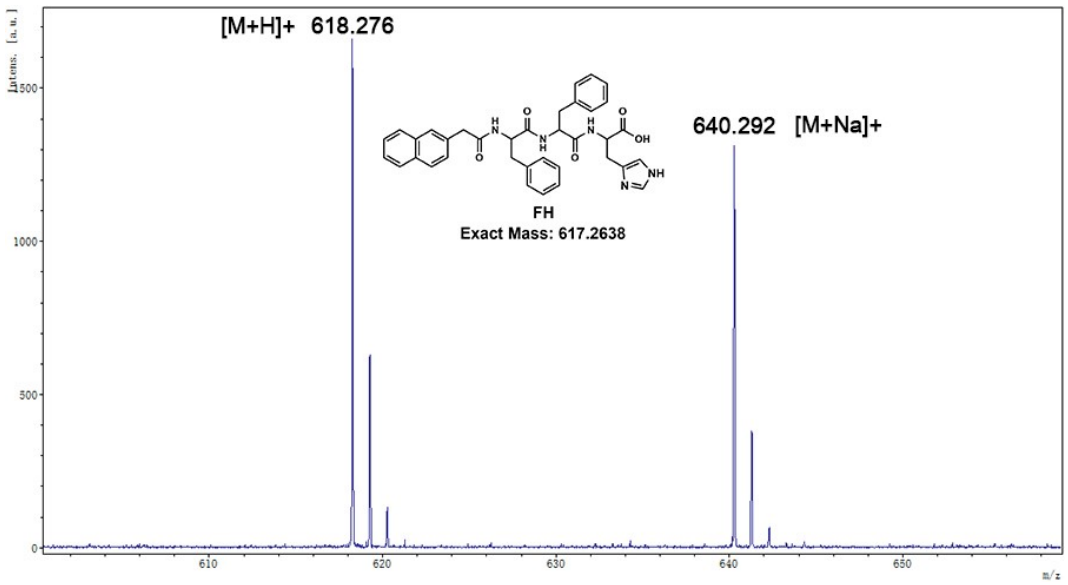


**Fig. S8.** MALDI-TOF mass spectrum of FH.

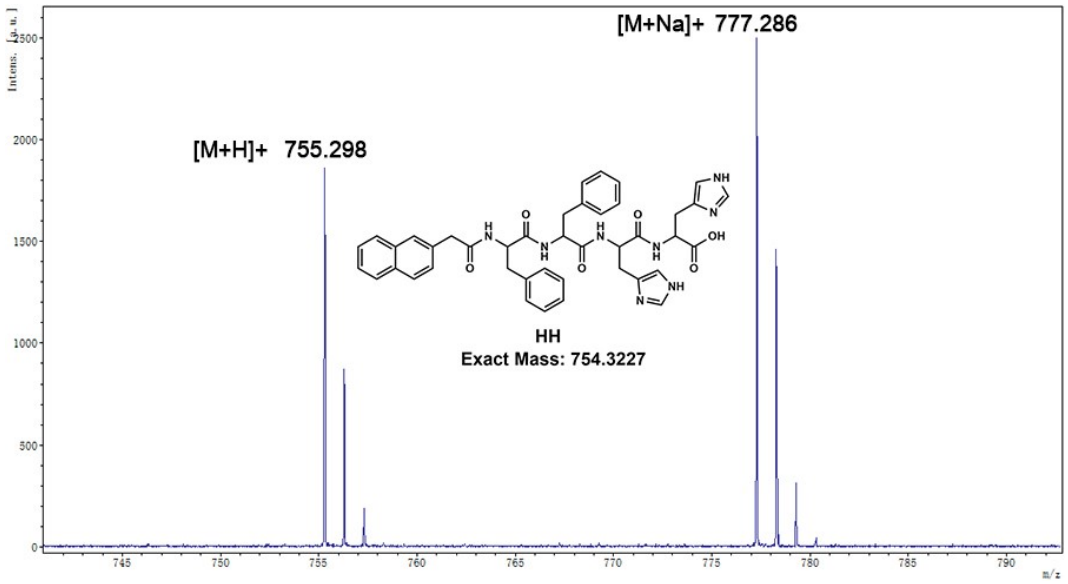


**Fig. S9.** MALDI-TOF mass spectrum of HH.

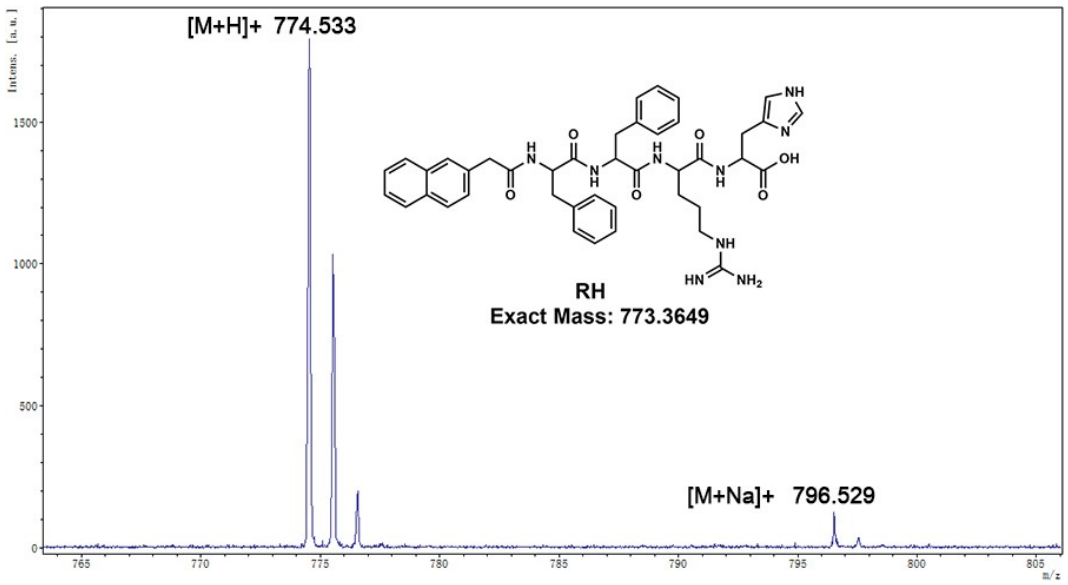


**Fig. S10.** MALDI-TOF mass spectrum of RH.

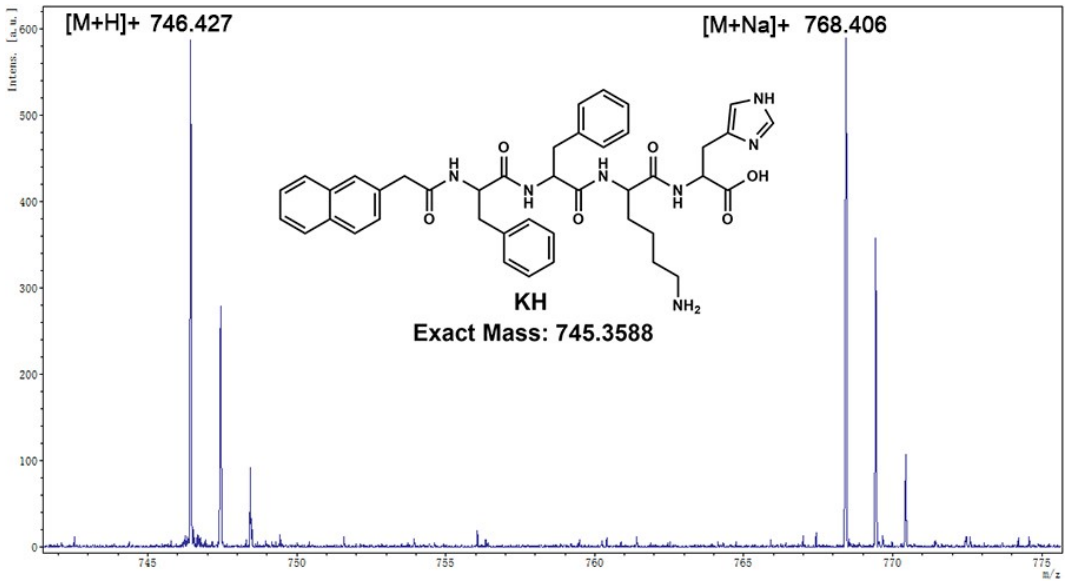


**Fig. S11.** MALDI-TOF mass spectrum of KH.

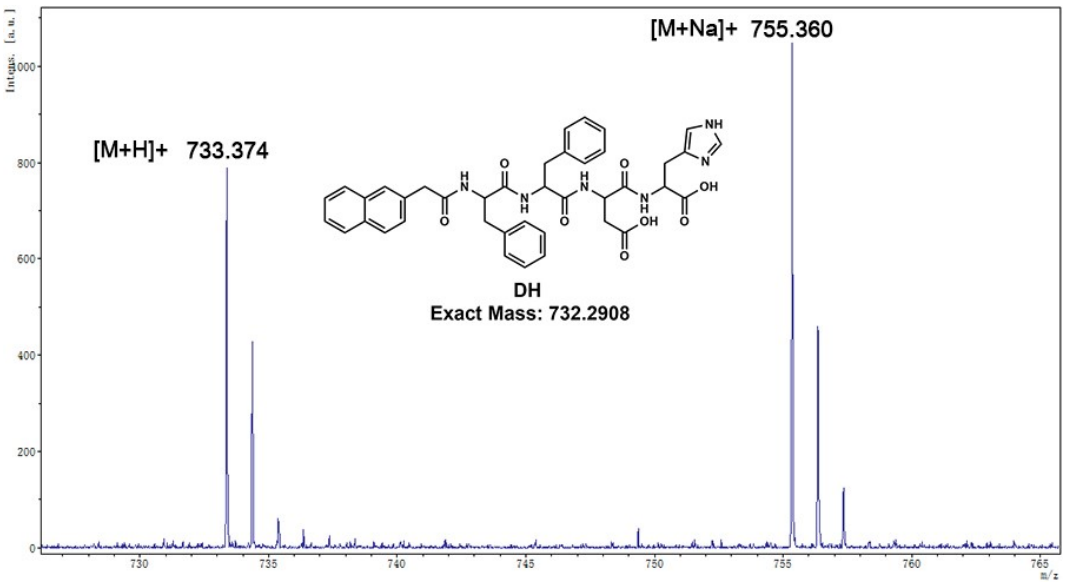


**Fig. S12.** MALDI-TOF mass spectrum of DH.

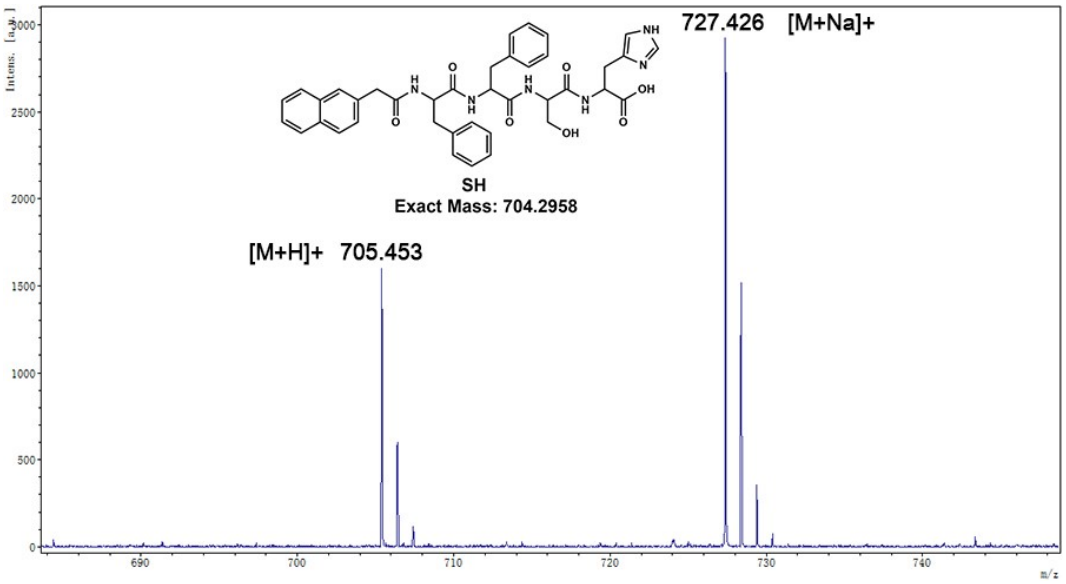


**Fig. S13.** MALDI-TOF mass spectrum of SH.

## 4. Rheological measurements of peptide hydrogels

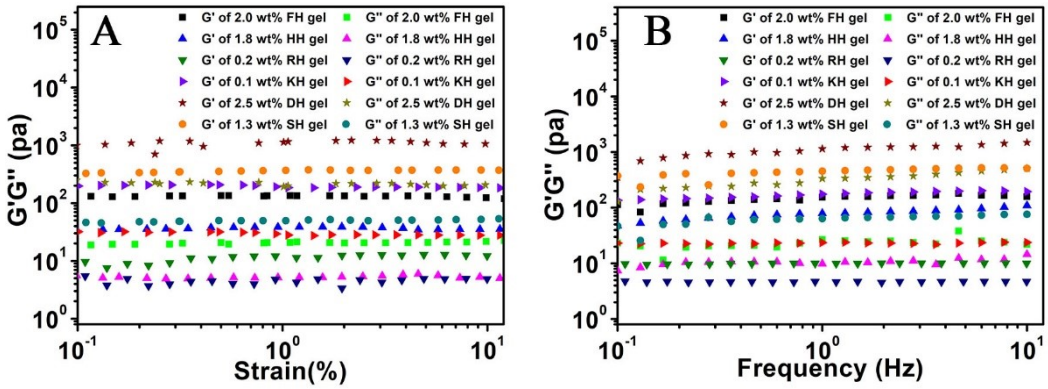

**Fig. S14.** (A) Strain dependence and (B) frequency dependence of the dynamic storage moduli (G') and the loss moduli (G'') of histidine-containing peptides.

## 5. Determination of the critical self-assembling concentration of peptides

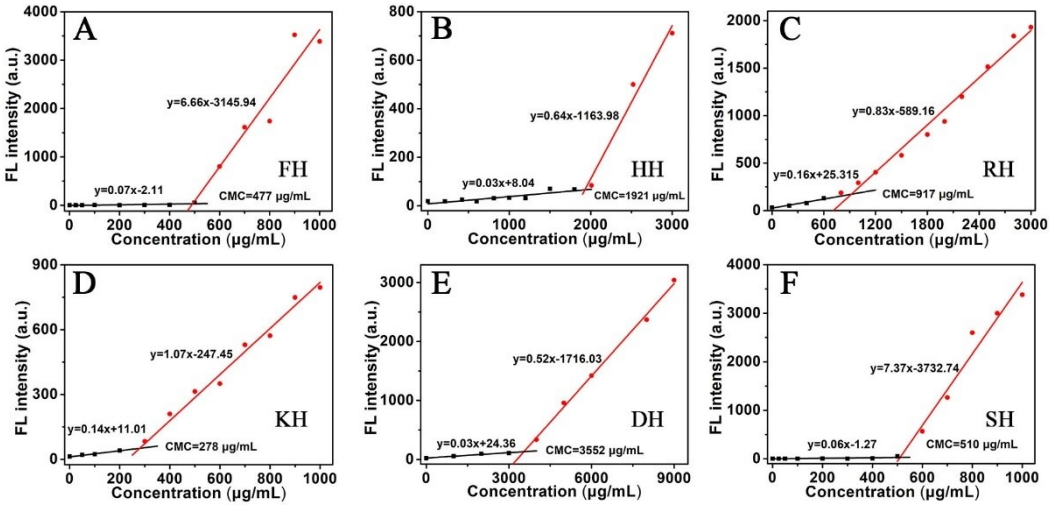


**Fig. S15.** The dose-dependent curves plotted with fluorescence intensities of Thioflavin T ($2.0 \times 10^{-5}$ M) versus varied concentrations of peptides.

## 6. Steady state kinetic analysis of hydrolase-like activities of self-assembling peptides

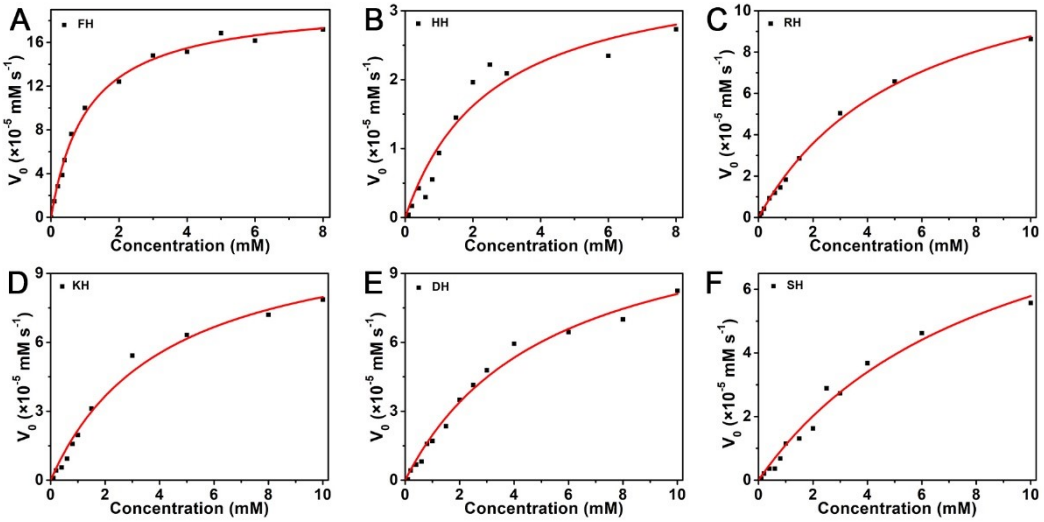


**Fig. S16.** (A-F) Michaelis-Menten curves for the hydrolysis of *p*-NPA (0.2, 0.4, 0.6, 0.8, 1.0, 2.0, 4.0, 6.0, 8.0 and 10.0 mM) by histidine-containing peptides (0.1 mM).

**Table S1.** Apparent kinetic parameters ($k_{cat}$, $K_M$ and ($k_{cat}/K_M$) for the hydrolysis of *p*-NPA catalyzed by different catalytic peptides in 10 mM PBS buffer under 25 ℃

| | $V_{max}$ ($\times 10^{-5}$ mM $s^{-1}$) | $K_M$ (mM) | $k_{cat}$ ($\times 10^{-3}$ $s^{-1}$) | $k_{cat}$ / $K_M$ ($M^{-1}$ $s^{-1}$) |
|---|---|---|---|---|
| FH | 19.61 | 0.93 | 1.96 | 2.11 |
| HH | 3.69 | 2.56 | 0.37 | 0.14 |
| RH | 13.74 | 5.68 | 1.37 | 0.24 |
| KH | 11.32 | 4.19 | 1.13 | 0.27 |
| DH | 12.42 | 5.32 | 1.24 | 0.23 |
| SH | 10.88 | 8.80 | 1.01 | 0.12 |

**Table S2.** Kinetic parameters for *p*-NPA hydrolysis by FH at different concentrations

| FH (mM) | $V_{max}$ ($\times 10^{-5}$ mM $s^{-1}$) | $K_M$ (mM) | $k_{cat}$ ($\times 10^{-3}$ $s^{-1}$) | $k_{cat}$ / $K_M$ ($M^{-1}$ $s^{-1}$) |
|---|---|---|---|---|
| 0.1 | 19.61 | 0.93 | 1.96 | 2.11 |
| 0.2 | 38.10 | 1.03 | 1.91 | 1.85 |
| 0.4 | 77.50 | 0.93 | 1.94 | 2.09 |

## 7. CD spectra of peptide-$Cu^{2+}$ complexes

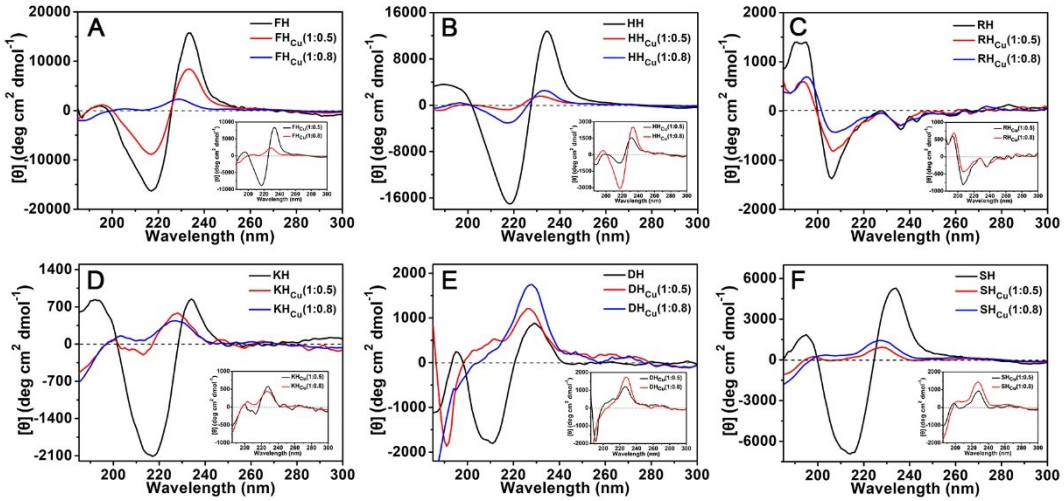


**Fig. S17** CD spectra of histidine-containing peptides (5.0 mM) and peptide-$Cu^{2+}$ complexes (5.0 mM) in PBS buffer (10 mM).

## 8. FT-IR spectra of peptide-$Cu^{2+}$ complexes

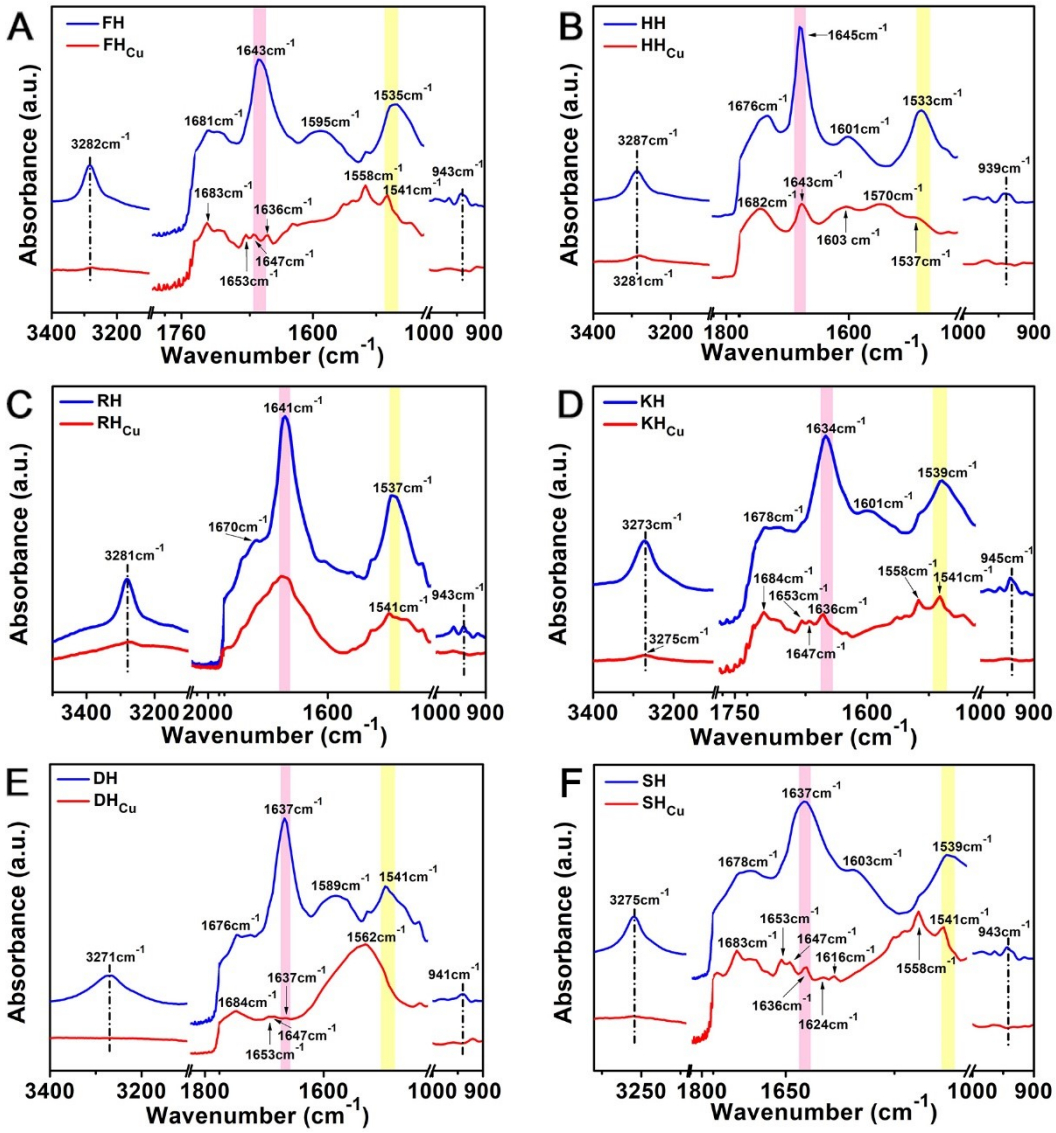


**Fig. S18.** FT-IR spectra of histidine-containing peptides (5.0 mM) and peptide-$Cu^{2+}$ complexes (5.0 mM) in PBS buffer (10 mM). The mole ratio of peptides to $Cu^{2+}$ ions was 1 : 0.8.

## 9. MALDI-TOF mass spectra of peptide-$Cu^{2+}$ complexes

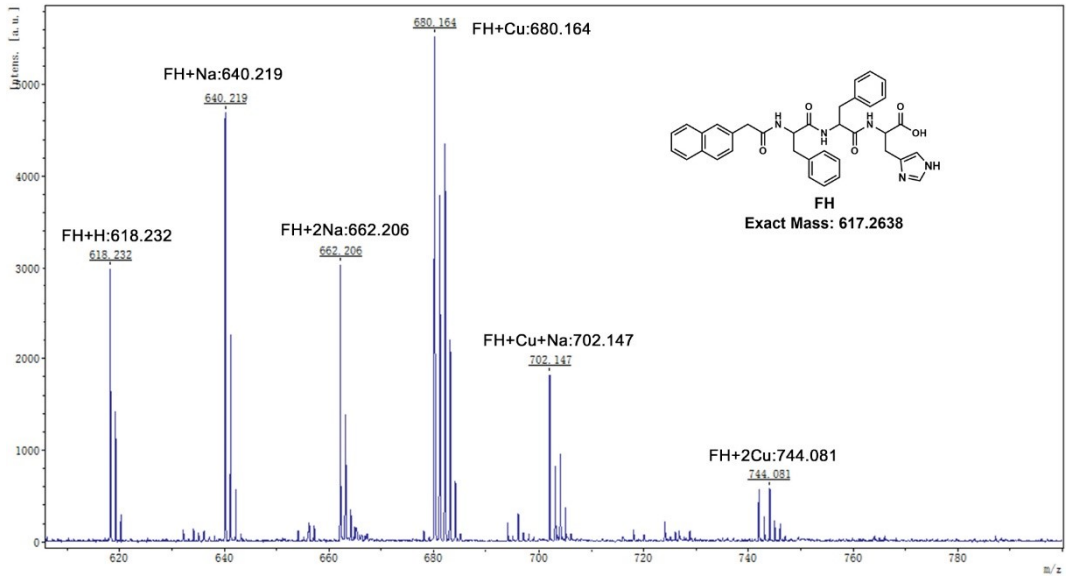


**Fig. S19.** MALDI-TOF mass spectrum of $FH_{Cu}$.

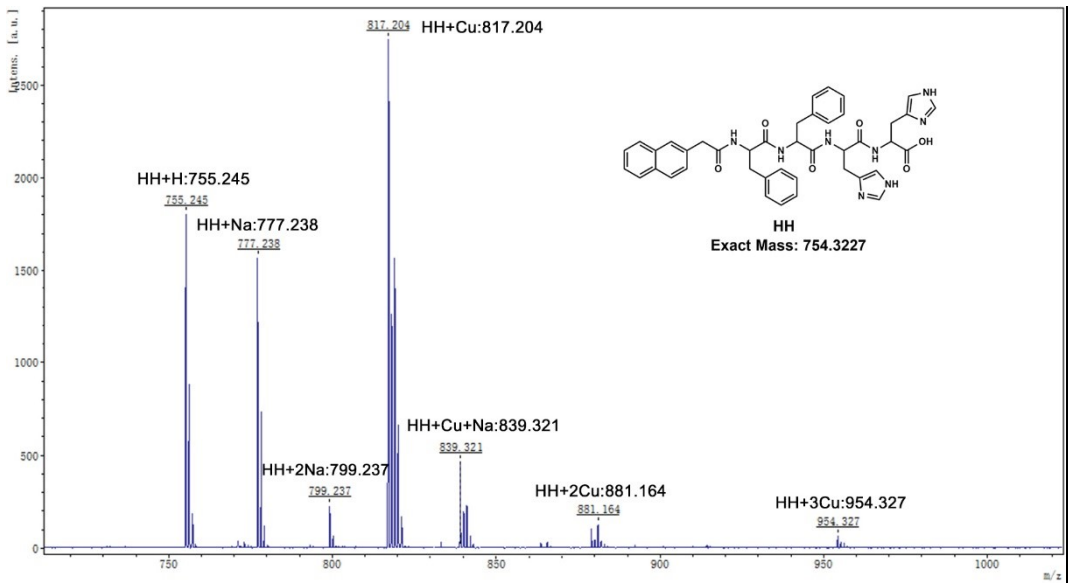


**Fig. S20.** MALDI-TOF mass spectrum of $HH_{Cu}$.

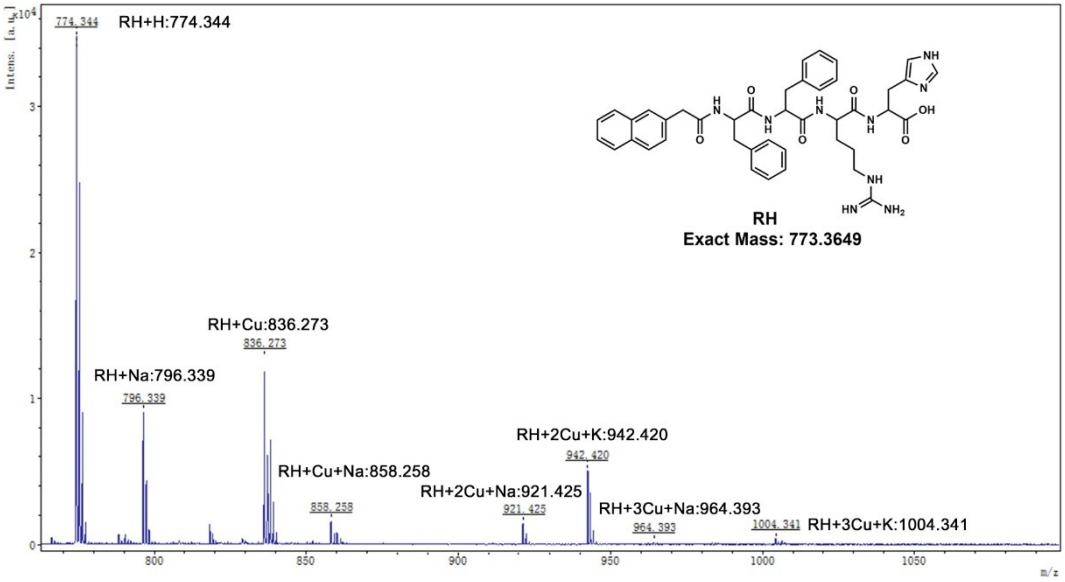


**Fig. S21.** MALDI-TOF mass spectrum of $RH_{Cu}$.

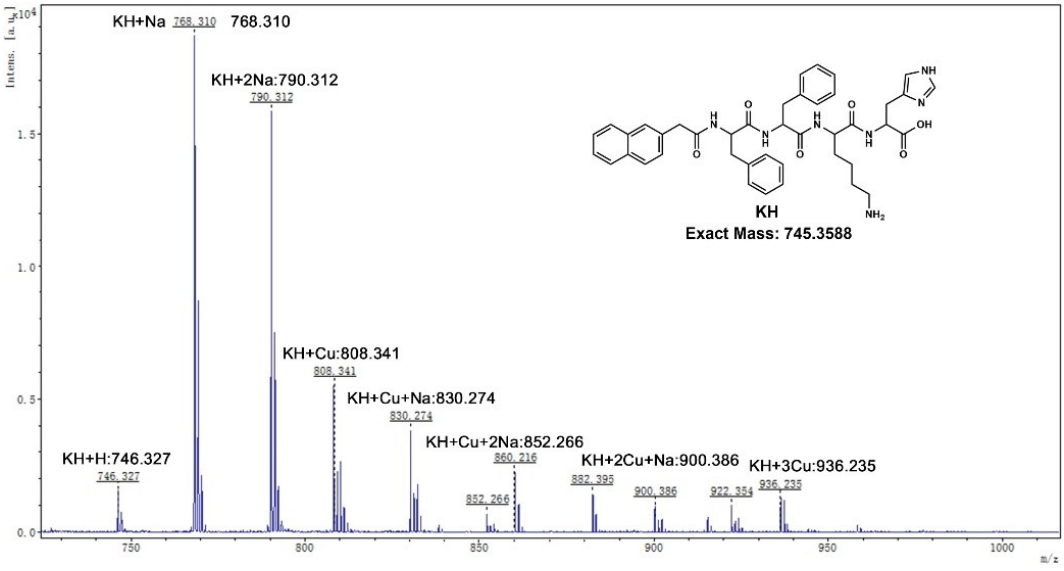


**Fig. S22.** MALDI-TOF mass spectrum of $KH_{Cu}$.

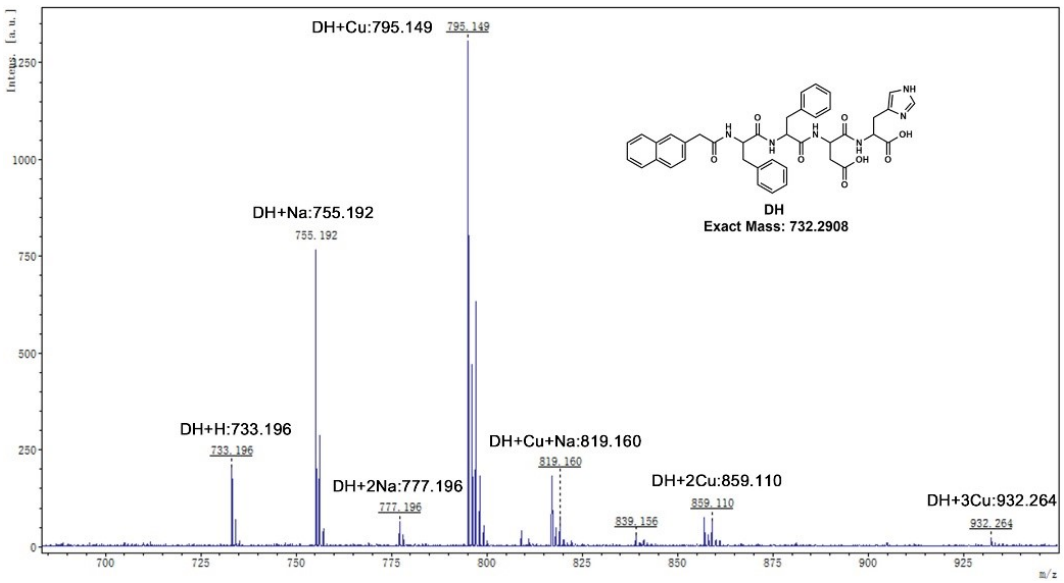


**Fig. S23.** MALDI-TOF mass spectrum of $DH_{Cu}$.

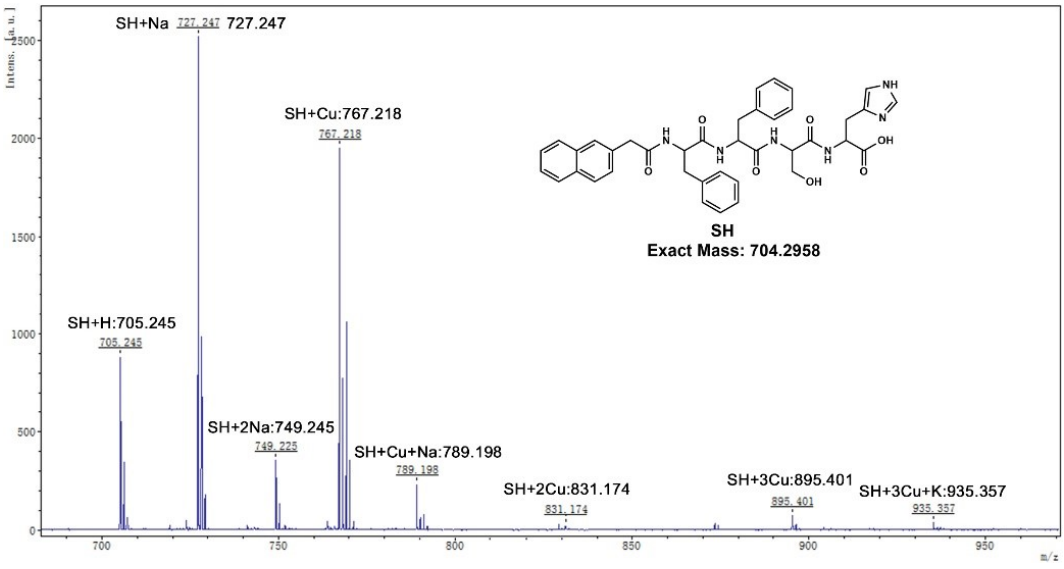


**Fig. S24.** MALDI-TOF mass spectrum of $SH_{Cu}$.

## 10. TEM images of histidine-containing peptides and peptide-$Cu^{2+}$ complexes

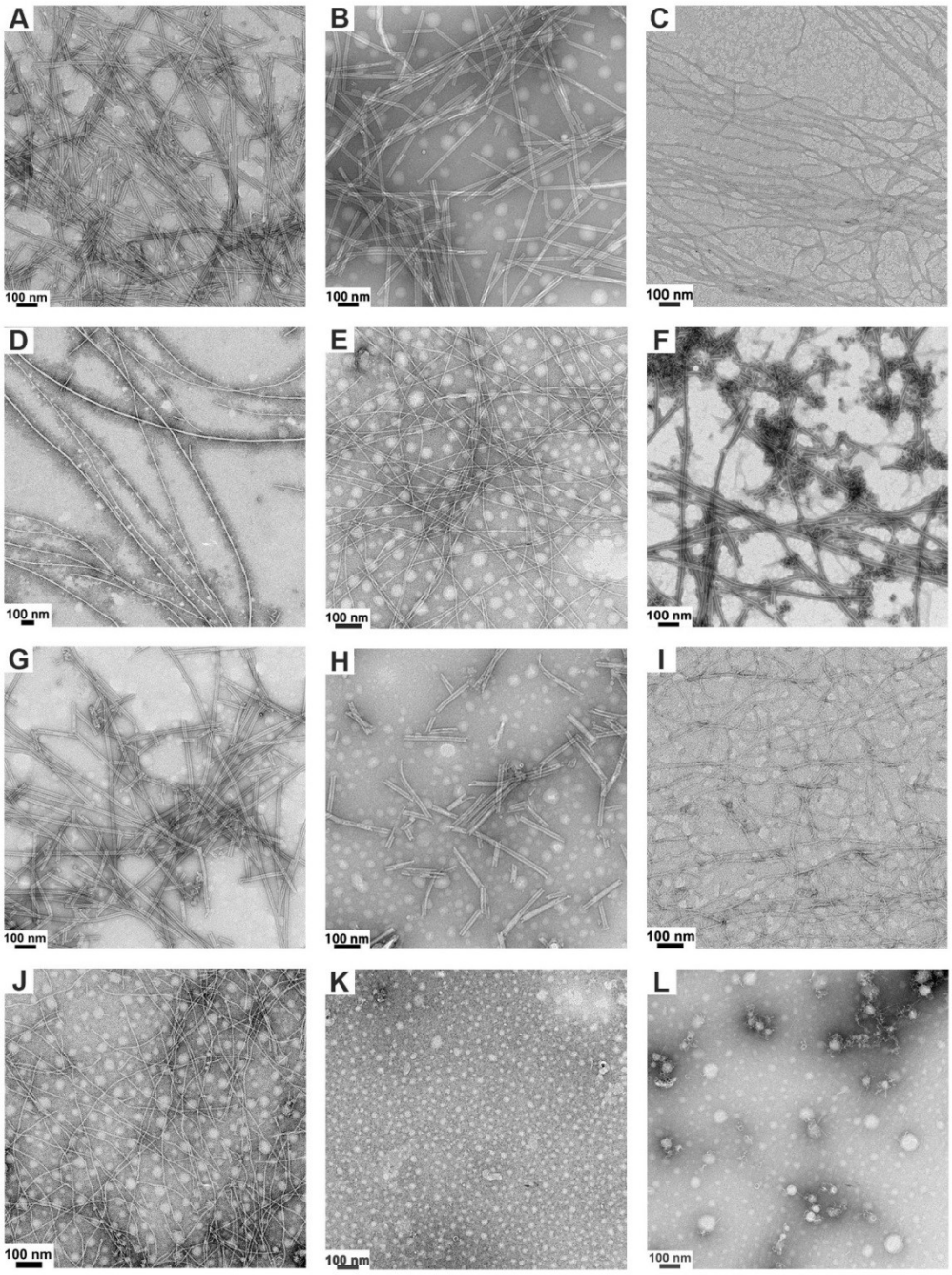


**Fig. S25.** TEM images of self-assembled nanostructures within hydrogels of histidine-containing peptides (Images of A-F represent FH, HH, RH, KH, DH and SH, respectively) and peptide-$Cu^{2+}$ complexes (Images of G-L represent $FH_{Cu}$, $HH_{Cu}$, $RH_{Cu}$, $KH_{Cu}$, $DH_{Cu}$ and $SH_{Cu}$, respectively).

**11. Hydrolysis of *p*-NPA by $FH_{Cu}$**

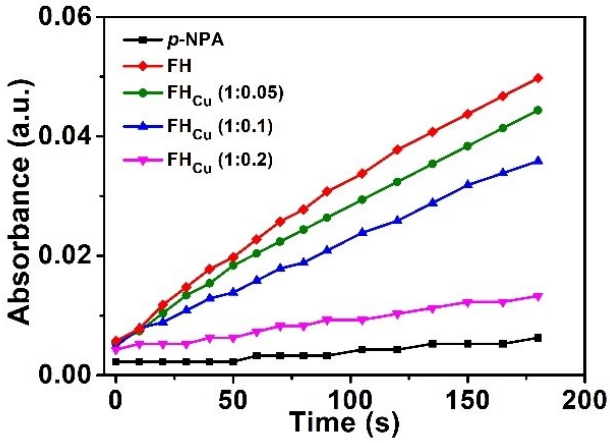


**Fig. S26.** Catalytic activities of $FH_{Cu}$ for the hydrolysis of *p*-NPA, [FH] = 0.1 mM, [*p*-NPA] = 0.5 mM. The mole ratio of FH to $Cu^{2+}$ ions was set as 1 : 0.05, 1 : 0.1, 1 : 0.2.

**12. Optical images of different solutions for TMB oxidation**

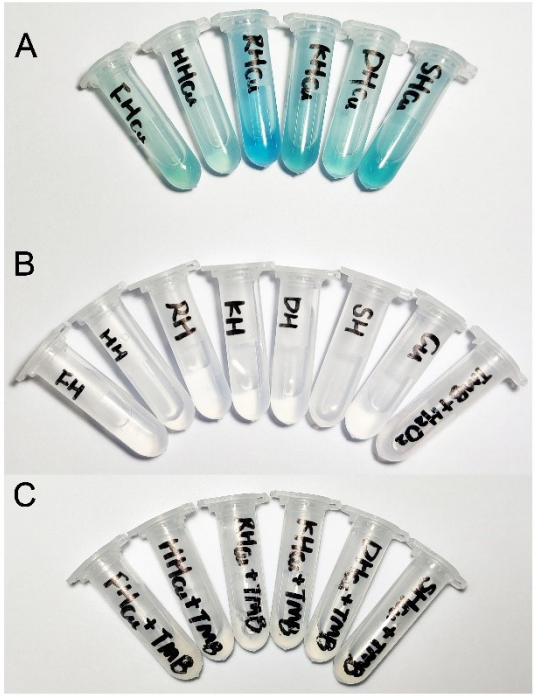


**Fig. S27.** Optical images of different test solutions for TMB oxidation. (A) Different sample solutions containing 0.4 mM of peptide-$Cu^{2+}$ complexes, 0.3 mM of TMB and 2.0 mM of $H_2O_2$ for the oxidation of TMB at 25 ℃. (B) Different sample solutions containing 0.4 mM of peptides, 0.3 mM of TMB and 2.0 mM of $H_2O_2$. (C) Sample

solutions 0.4 mM of peptide-$Cu^{2+}$ complexes, 0.3 mM of TMB, but without $H_2O_2$. The mole ratio of peptide to $Cu^{2+}$ ions was 1 : 1.

**13. Peroxidase-like catalytic activities of peptide-$Cu^{2+}$ complexes**

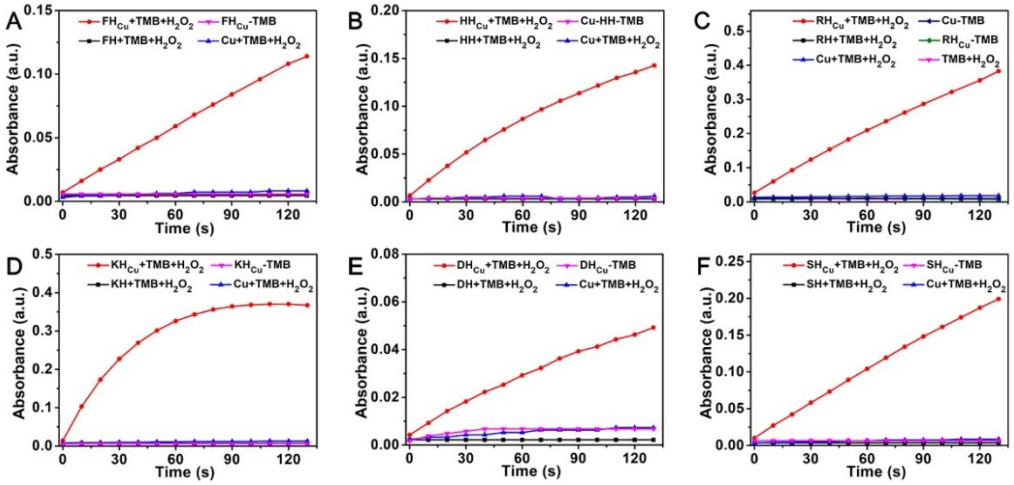


**Fig. S28.** Time dependent absorbance at 640 nm for the oxidization of TMB catalysed by different peptide-$Cu^{2+}$ complexes in 10 mM PBS buffer (pH 7.4) at 25 ℃, (A) TMB + $H_2O_2$; (B) peptide-$Cu^{2+}$ + TMB + $H_2O_2$; (C) $Cu^{2+}$ + TMB + $H_2O_2$; (D) peptide + TMB + $H_2O_2$; (E) peptide-$Cu^{2+}$ + TMB; (F) $Cu^{2+}$ + TMB. Reaction conditions: [peptide-$Cu^{2+}$] = 0.4 mM, [$Cu^{2+}$] = 0.4 mM, [TMB] = 0.3 mM, [$H_2O_2$] = 3.0 mM, and the mole ratio of peptide to $Cu^{2+}$ ions was 1 : 1.

**14. Effects of metal ions on the catalytic activity of peptide-metal complexes**

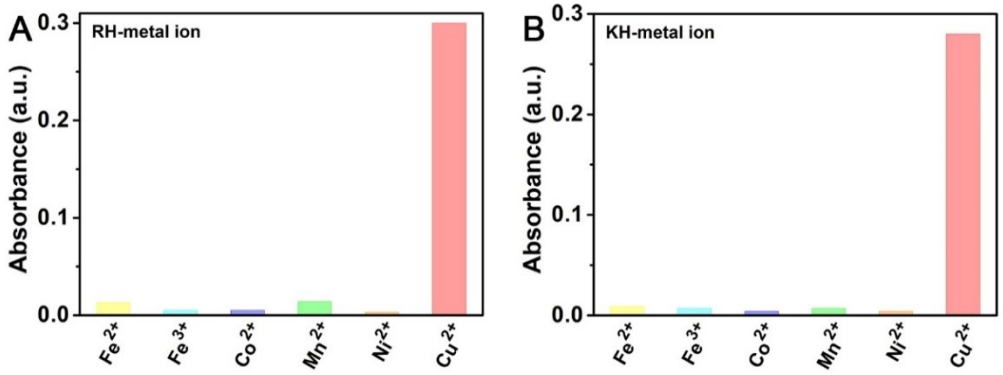


**Fig. S29.** Effects of metal ions on the catalytic activity of peptide-metal complexes. (A) RH-metal + TMB + $H_2O_2$; (B) KH-metal + TMB + $H_2O_2$. Reaction conditions: [peptide-metal] = 0.4 mM, [TMB] = 0.2 mM, [$H_2O_2$] = 5.0 mM, and the mole ratio of peptide to metal ions was 1 : 0.8.

**15. Determination of the optimum ratio of peptides to $Cu^{2+}$ ions**

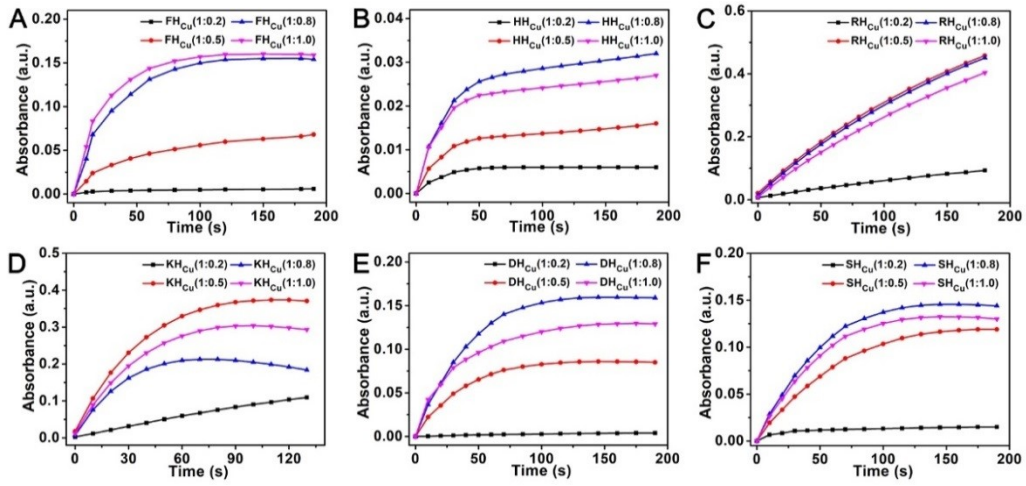


**Fig. S30.** Time dependent absorbance at 640 nm for the oxidization of TMB catalyzed by peptide-$Cu^{2+}$ complexes in different ratios of peptides to $Cu^{2+}$ ions. (A) $FH_{Cu}$ + TMB + $H_2O_2$; (B) $HH_{Cu}$ + TMB + $H_2O_2$; (C) $RH_{Cu}$ + TMB + $H_2O_2$; (D) $KH_{Cu}$ + TMB + $H_2O_2$; (E) $DH_{Cu}$ + TMB + $H_2O_2$; (F) $SH_{Cu}$ + TMB + $H_2O_2$. Reaction conditions: [peptide-$Cu^{2+}$] = 0.4 mM, [TMB] = 0.2 mM, [$H_2O_2$] = 5.0 mM, and the inset showed the mole ratio of peptides to $Cu^{2+}$ ions.

**16. Determination of reactive oxygen species involved in the process of TMB oxidation (按手稿描述，将 16 和 17 调换顺序)**

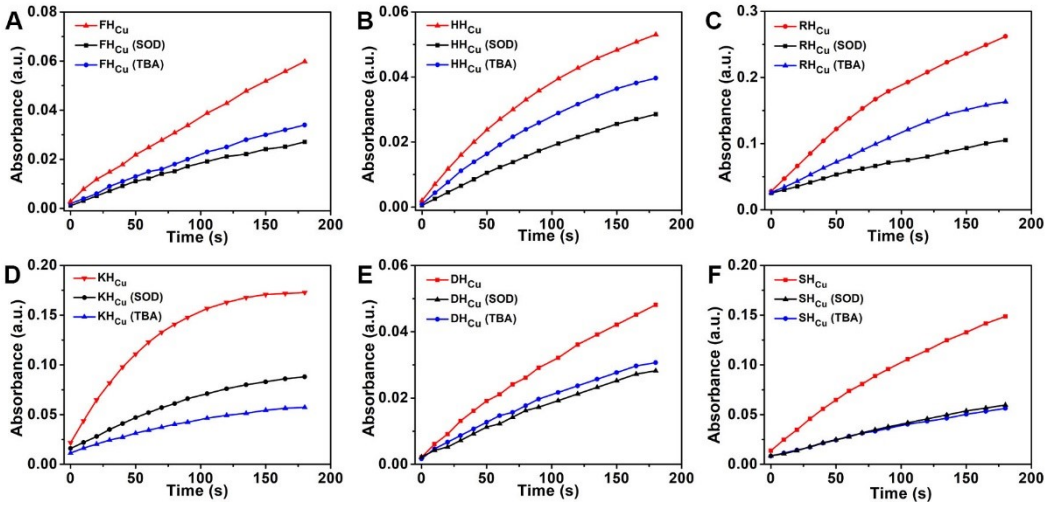


**Fig. S31.** Determination of reactive oxygen species involved in the process of TMB oxidation in 10 mM PBS buffer (pH 7.4) at 25 ℃. (A) $FH_{Cu}$ + TMB + $H_2O_2$ + SOD / TBA; (B) $HH_{Cu}$ + TMB + $H_2O_2$+ SOD / TBA; (C) $RH_{Cu}$ + TMB + $H_2O_2$ + SOD /

TBA; (D) $KH_{Cu}$ + TMB + $H_2O_2$ + SOD / TBA; (E) $DH_{Cu}$ + TMB + $H_2O_2$+ SOD / TBA; (F) $SH_{Cu}$ + TMB + $H_2O_2$+ SOD / TBA. Reaction conditions: [peptide-$Cu^{2+}$] = 0.4 mM, [TMB] = 0.2 mM, [$H_2O_2$] =1.0 mM, [SOD] = 60 μM, [TBA] = 60 mM, and the mole ratio of peptide to $Cu^{2+}$ ions was 1 : 0.8.

**17. Steady-state kinetics assays of peptide-$Cu^{2+}$ complexes**

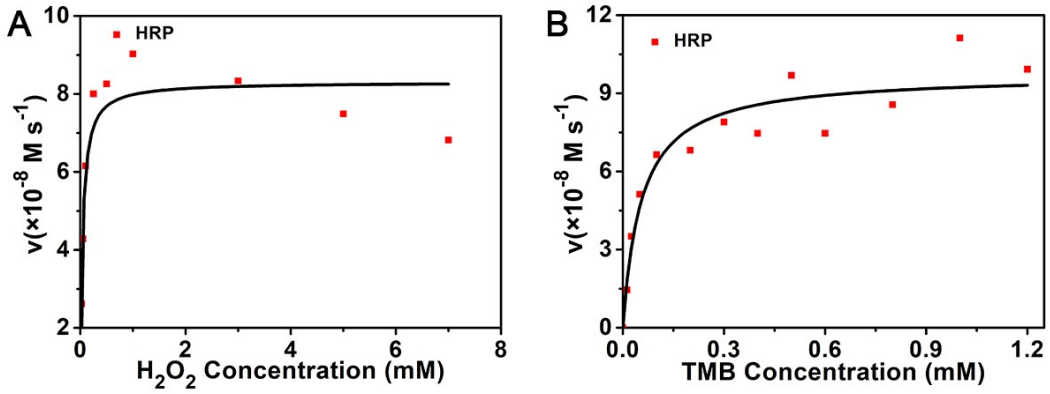


**Fig. S32** Steady-state kinetic assays of HRP for the oxidation of TMB. The velocity ($v$) of the reaction was measured using $10^{-6}$ mM HRP in 1 mL of $1.0\times10^{-2}$ M PBS buffer (pH 7.4) at 25 ℃. (A) The Michaelis-Menten curve of HRP for the oxidation of TMB by fixing the TMB concentration at 0.4 mM and varying $H_2O_2$ concentrations. (B) The Michaelis-Menten curve of HRP for the oxidation of TMB by fixing the $H_2O_2$ concentration at 3.0 mM and varying TMB concentrations.

**Table S3.** Kinetic parameters of TMB oxidation by peptide-$Cu^{2+}$ complexes and HRP

| Catalyst | Substrate | $K_M$ (mM) | $V_{max}$ (×$10^{-8}$ M $s^{-1}$) | $k_{cat}$ ($s^{-1}$) | $k_{cat}$ / $K_M$ ($M^{-1}$ $s^{-1}$) |
|---|---|---|---|---|---|
| **$FH_{Cu}$** | TMB | 0.77 | 6.76 | $3.38\times10^{-4}$ | 0.44 |
| **$FH_{Cu}$** | $H_2O_2$ | 7.77 | 5.22 | $2.61\times10^{-4}$ | 0.03 |
| **$HH_{Cu}$** | TMB | 4.32 | 22.6 | $11.3\times10^{-4}$ | 0.26 |
| **$HH_{Cu}$** | $H_2O_2$ | 4.84 | 7.76 | $3.88\times10^{-4}$ | 0.08 |
| **$RH_{Cu}$** | TMB | 0.40 | 10.80 | $5.40\times10^{-4}$ | 1.35 |
| **$RH_{Cu}$** | $H_2O_2$ | 2.32 | 19.02 | $9.51\times10^{-4}$ | 0.41 |
| **$KH_{Cu}$** | TMB | 1.28 | 53.36 | $26.68\times10^{-4}$ | 2.08 |
| **$KH_{Cu}$** | $H_2O_2$ | 1.11 | 34.80 | $17.40\times10^{-4}$ | 1.57 |

| | | | | | |
|---|---|---|---|---|---|
| **$DH_{Cu}$** | TMB | 1.90 | 5.52 | $2.76\times10^{-4}$ | 0.15 |
| **$DH_{Cu}$** | $H_2O_2$ | 7.61 | 4.02 | $2.01\times10^{-4}$ | 0.03 |
| **$SH_{Cu}$** | TMB | 0.79 | 11.2 | $5.06\times10^{-4}$ | 0.64 |
| **$SH_{Cu}$** | $H_2O_2$ | 16.22 | 22.32 | $11.16\times10^{-4}$ | 0.07 |
| **HRP** | TMB | 0.055 | 9.73 | 97.3 | $1.78\times10^{6}$ |
| **HRP** | $H_2O_2$ | 0.040 | 8.30 | 83.0 | $2.08\times10^{6}$ |

## 18. Biostability tests of peptides and peptide-$Cu^{2+}$ complexes

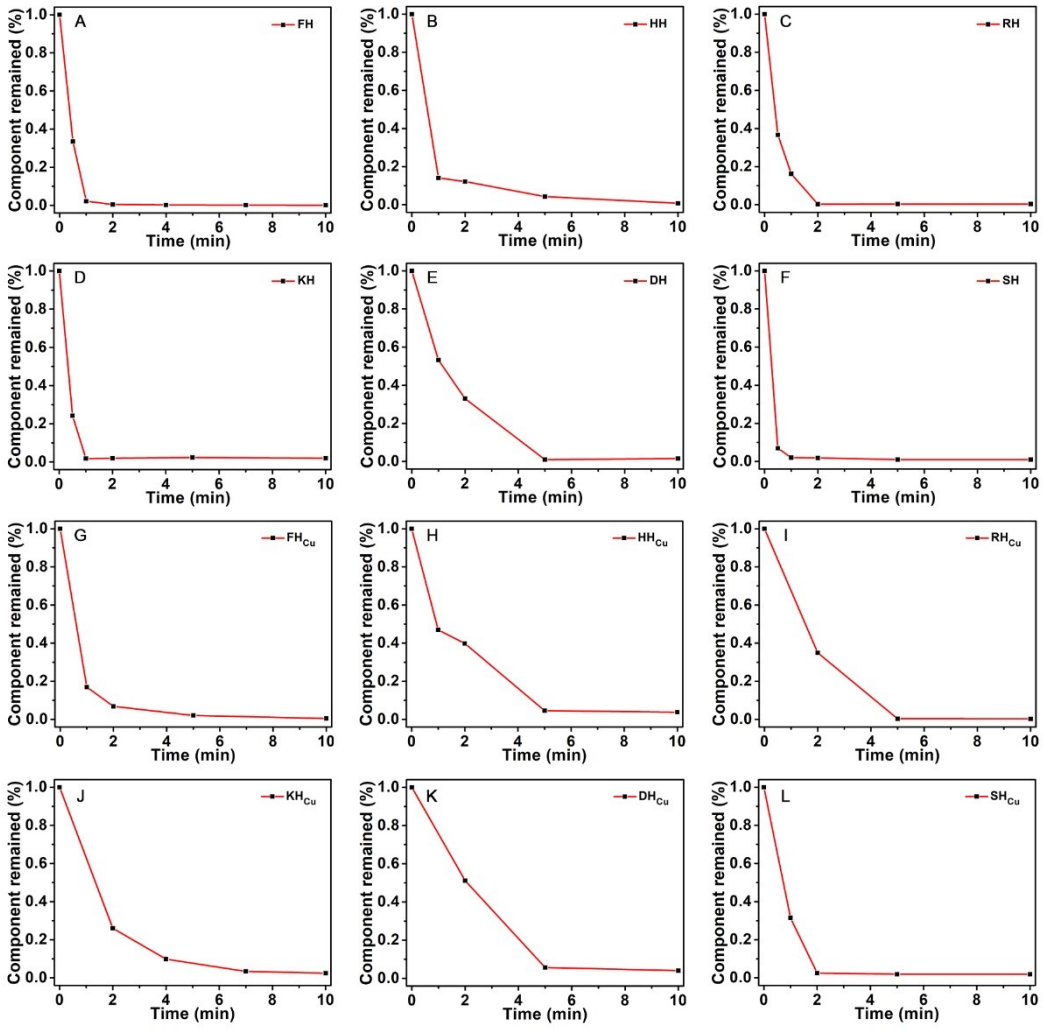


**Fig. S33.** Quantitative data about the degradation ratio of (A-F) different peptides (FH, HH, RH, KH, DH and SH), and (G-L) their corresponding peptide-$Cu^{2+}$ complexes ($FH_{Cu}$, $HH_{Cu}$, $RH_{Cu}$, $KH_{Cu}$, $DH_{Cu}$ and $SH_{Cu}$ ) by proteinase K (3.2 units/mL) at 37 ℃.

## 19. The viabilities of HUVECs treated by KH and $KH_{Cu}$

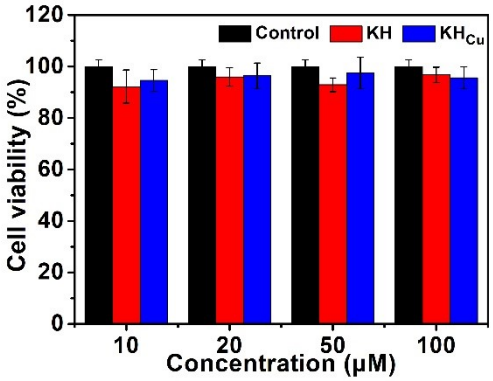


**Fig. S34.** Cytotoxicity tests of KH, and the corresponding $Cu^{2+}$ complex ($KH_{Cu}$) towards HUVEC cells over the course of 24 h.